Applied Surface Science 679 (2025) 161115

Contents lists available at ScienceDirect

Applied Surface Science

journal homepage: www.elsevier.com/locate/apsusc

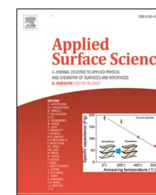

Full Length Article

Cleaning of laser-induced periodic surface structures on copper by gentle wet chemical processing

Pierre Lorenz [a], Martin Ehrhardt [a], Andriy Lotnyk [a], Jan Griebel [a], Klaus Zimmer [a], Joachim Zajadacz [a,*], Marcel Himmerlich [b], Elena Bez [b,c], Mauro Taborelli [b], Steffen Rosenow [d], Ronny Tepper [d], Alexander Max Breul [d,**]

[a] Leibniz Institute of Surface Engineering (IOM), Permoserstraße 15, 04318 Leipzig, Germany
[b] CERN (European Organization for Nuclear Research), 1211 Geneva 23, Switzerland
[c] Faculty of Physics and Earth System Science, University of Leipzig, Linnéstraße 5, 04103 Leipzig, Germany
[d] Intelligent Fluids GmbH, Karl-Heine-Straße 99, 04229 Leipzig, Germany

ARTICLE INFO

Keywords:
Laser ablation
Laser-induced periodic surface structures (LIPSS)
Debris
Wet-chemical etching
Cleaning

ABSTRACT

Laser-induced periodic surface structures (LIPSS) attract considerable attention due to the manifold applications enabled by these self-organised structures ranging from optical colouring to bio-mimicking or wetting effects. The mechanism of LIPSS-formation at metal surfaces includes laser-ablation processes that results in phase transitions, explosive material removal and partial redeposition of the ablation products in the form of nanoscopic debris or even sub-micrometre-sized spherical particles in case of melt ejection. For some applications, these particulates, debris, and microscopic features on top of the periodic surface structures are disadvantageous. We studied wet-chemical cleaning approaches to remove redeposited material from LIPSS to enhance their applicability. LIPSS on copper with a lateral periodicity of ~ 365 nm, that were fabricated by ultrashort pulse laser exposure (λ: 515 nm, t_p: 260 fs), were cleaned with different liquids ranging from solvents to microemulsions. The surface morphologies were characterised by scanning electron microscopy (SEM), atomic force microscopy (AFM) and transmission electron microscopy (TEM) to study the surface topography, the size and density of surface particulates as well as other surface contaminations before and after wet cleaning. The LIPSS surface composition was analysed by X-ray photoelectron spectroscopy (XPS), Raman spectroscopy and Energy-dispersive x-ray spectroscopy (EDX) at the FIB-cross sections. The different cleaning approaches are classified with respect to their capability to remove particles and contaminations as well as to their influence on the morphology and shape of LIPSS pattern, whereby substantial differences are found. At least two wet-chemical solutions enable the removal of nanoparticles with only minor modification of the LIPSS topography. The main effect of wet cleaning is the detachment of particulates including sub-micrometre-sized spheres due to a gentle and selective etching of the interface region between the LIPSS and the redeposited material that comprise of modified copper and copper oxides.

1. Introduction

Laser-based micromachining of surfaces with laser ablation includes explosive processes of material removal that cause at one hand the formation of micro-patterns, but on the other hand also result in the partial redeposition of the ablated material on the treated surface. This material that is often called debris is redeposited around the laser spot and consist of various nanomaterials that include components of the substrate and the surrounding atmosphere. The spontaneous formation of self-organized surface structures at different length-scales is linked to chemical and physical surface processes. Such self-organizing processes can be initiated by exposure of surfaces to energetic beams and are well known as laser-induced periodic surface structures (LIPSS) or as ripples for ion beam processing [1,2]. In relation to the normalized period and the formation mechanism, low- and high-spatial frequency (LSFL and HSFL) LIPSS can be distinguished [1].

* Corresponding author at: Leibniz Institute of Surface Engineering (IOM), Permoserstraße 15, 04318 Leipzig, Germany.
** Corresponding author at: Intelligent fluids GmbH, Karl-Heine-Straße 99, 04229 Leipzig, Germany.
E-mail addresses: joachim.zajadacz@iom-leipzig.de (J. Zajadacz), breul@intelligent-fluids.com (A.M. Breul).

https://doi.org/10.1016/j.apsusc.2024.161115
Received 3 June 2024; Received in revised form 23 August 2024; Accepted 28 August 2024
Available online 31 August 2024
0169-4332/© 2024 The Author(s). Published by Elsevier B.V. This is an open access article under the CC BY-NC-ND license (http://creativecommons.org/licenses/by-nc-nd/4.0/).

The LIPSS results from the interference of incidence and scattered laser radiation close to the surface. Their formation has been extensively studied for copper surfaces using ultrashort laser pulses investigating the influence of laser parameters such as wavelength, pulse duration, and laser fluence [3–6]. In addition to ablative LIPSS formed in copper, additional nanostructures can result from melting and laser-ablation-induced redeposition effects [7]. Hence, LIPSS are often decorated by nanoparticles or spherical particulates as a consequence of melting and ablative processes [8]. Reliable cleaning procedures that keep the LIPSS structures intact are currently not available [9].

The challenges of debris removal at laser ablation processing is an everlasting problem that can be tackled by removing ablation products before being redeposited at the surface, e.g. by exhaust, gas streams or enhanced gas phase transport conditions [10]. Furthermore, post-processing approaches for surface cleaning by wet-chemical or physical techniques are possible. For example, wet cleaning of laser ablated diamond films has been performed under harsh conditions that cannot be applied to copper as the LIPSS pattern would be immediately destroyed by the etchant [11].

The cleaning of surfaces including the removal of additional particles is well known for semiconductor surfaces and is optimized for various materials and processes [12]. Two cleaning mechanisms are usually applied: (i) wet chemical cleaning that often includes gentle etching and/or sonication as well as (ii) dry chemical or physical cleaning. The most suitable method for a particular cleaning problem depends on the type of contamination (particles or film-like, organic or/and inorganic), the interaction nature of the contaminations with the surface, and the potential surface damages induced by the cleaning techniques. The particle–surface interaction can depend on the presence of van der Waals, double layer, or electrostatic forces, while even more complex adhesion mechanisms can exist for biological particles [13].

Laser-assisted cleaning with and without water support or a humid ambient has been studied for wafer processing. Pulsed laser-driven techniques (often assisted by water) based on thermo-mechanical processes such as thermal expansion or shock wave generation have also be demonstrated to provoke the detachment of particles from surfaces [14–16].

Wet-chemical cleaning without mechanical support (e. g. sonication) rely on gentle or selective chemical etching. In the case of silicon wafer cleaning, highly selective etching processes can be utilized, e.g. the removal of silicon dioxide at the surface of silicon wafers using hydrofluoric acid [13]. Such a dissolution of surface layers allows the removal of adherent particles without etching the particles.

Cleaning of LIPSS on silicon or silicon compounds by wet-chemical etching improves the laser-fabricated pattern quality. Thereby, the well-known dependencies of the etching rate on the composition as well as the structure of material found close to the LIPSS are utilized for process specification. The selective etching of the amorphous phase of LIPSS in silicon in a KOH-based etchant has been used to realize homogeneous LIPSS with almost no remaining particulates. The depth of the LIPSS further increases with etching time to 260 nm whereas the LIPSS period is constant, thus enabling higher aspect ratios [17]. The cleaning of HSFL in SiC has been shown as a result of the selective etching of the laser-induced formed SiC degradation products with a standard silicon etchant [18].

Furthermore, also the wet-chemical cleaning from particles and passivation of unstructured copper was studied for different applications [19,20].

In general, aqueous wet cleaning conditions can be subdivided to basic, acidic, and neutral cleaning mechanisms. Due to its high tendency to complex formation in caustic aqueous media, e.g. by reaction with amines, copper is very sensitive to corrosion. Also, acidic conditions for sensitive metal surface treatments are not applicable because of catalytic reactions to hydrogen under metal ion formation. Consequently, neutral conditions must be applied for Cu cleaning. Therefore, the removal of organic contaminants, e.g., polymer films, is carried out using solvents like NMP (N-Methylpyrrolidone) or DMSO (Dimethyl sulfoxide). However, inorganic Cu particles redeposited during LIPSS formation cannot be removed by dissolution in organic solvents.

The utilization of microemulsion systems is a promising approach to obtain very clean surfaces, and to successfully remove of particles from copper surfaces. (I) Microemulsions contain surfactants which support the detachment of particles from surfaces. (II) Microemulsions are water-based formulations wherein etching effects can support the surface cleaning effect of the surfactant. (III) Microemulsions contain a high organic content, which enables the fine-tuning of the caustic or acidic etching effects by their intrinsic capability to take up various additives (e.g. corrosion inhibitors) or by the choice of complex forming functionalities within the organic molecules. Hence, microemulsion systems feature a very low surface tension allowing an excellent wetting of very small features and particles on surfaces. Therefore, microemulsions are promising candidates for Cu cleaning [21,22]. The basic composition of the gentle etching solution contains an etchant dispersed in a microemulsion consisting of an aqueous, an oil and a surfactant phase that form microemulsions. [21].

Despite that nanoparticles can be useful, e.g. in nanocomposites, in several cases laser-generated particles need to be removed from surface for environmental, health, as well as technical reasons. The wet-chemical cleaning of laser-induced periodic surface structures at copper is the aim of this study with emphasis on removal of particulate contamination while maintaining the LIPSS structure, i.e. avoiding etching of the periodic LIPSS topography. LIPSS on Cu are a candidate for electron-cloud mitigation in particle accelerators via secondary electron yield reduction [23]. For such an application, any particles or particle agglomerates, that are loosely bound to the surfaces facing the particle beam, are a great risk if particles get attracted by or interact with the beam, which could lead to beam instabilities or a beam dump to protect the accelerator from radiation damage.

2. Experimental techniques and materials

Oxygen-free electronic grade copper sheets of 1 mm thickness were cut to a size of 20 × 20 mm^2 and cleaned from adherent particles and organic contaminations in an isopropanol/H_2O (50 %/50 %) solution by sonication for 10 min (9 l H_2O bath at 200 W). After drying in a nitrogen stream, the samples were laser-irradiated with the linearly polarised second harmonic of a fs laser with fixed laser parameters ($\lambda = 515$ nm, $f_{rep} = 500$ kHz, $\Delta t_p = 260$ fs, P=1.18 W).

LIPSS were fabricated by scanning the laser beam in parallel lines across the sample surface with a line spacing of $\Delta y = 10$ µm and a scanning speed of v = 75 mm/s using a galvanometer scanner (see Fig. 1). The laser was focussed with a f-theta lens of focal length of 165 mm resulting in a spot size with a Gaussian radius of $\omega_0 = 14$ µm. The average pulse number for LIPSS generation has been calculated to be $N_A = \frac{f_{rep} \bullet \pi \bullet \omega_0^2}{v \bullet \Delta y} = 410$. These parameters applied for LIPSS generation at

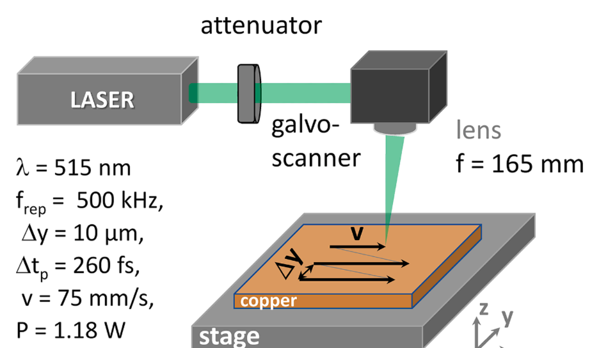

Fig. 1. Sketch of the experimental setup for LIPSS fabrication on copper samples and the machining strategy.

copper samples surface were intentionally not optimized for minimal particle density so that the redeposition of nanostructures, nanoparticles, and sub-micrometre-sized spheres occurs during fabrication.

Afterwards, the laser-processed Cu-surfaces were cleaned in different specific wet-chemical cleaning solutions (summarized in Table 1) with ultra-sonication for 5 min and 35 min at 25 °C. After wet-chemical cleaning, the samples were subsequently ultrasonicated in isopropanol / H_2O (1:1) at 50 °C for 5 min, then rinsed in isopropanol / H_2O solution and finally dried in a nitrogen stream.

For comparison (sample NGL) the protocol for cleaning of ultra-high vacuum components at CERN was applied. Degreasing by immersion in detergent DP 17.40 SUP (NGL) around 50 °C for approximately 2 h with ultrasonic for 15 min, followed by rinsing with demineralised water jet and immersion, spraying with ethanol, dry-blowing with compressed nitrogen, baking in hot air flow at 60 °C for up to 60 min, and finally cooling-down to room temperature.

The surfaces were examined by imaging and spectroscopic techniques to determine the surface morphology as well as their chemical composition. A SEM (Gemini Ultra 55, Zeiss) was used to inspect the sample surface in secondary electron imaging mode with high resolution. Atomic force microscopy (Dimension ICON; Bruker) was performed in tapping mode with a xy-closed loop configuration. An area of 3 µm x 3 µm was characterized acquiring 1024 × 1024 datapoints. The raw data were subjected to a plane correction consisting of a global plane fit and a line-wise correction subtracting a fitted polynomial function of the 3rd order from each scan line via SPIP™ software (version 6.0.14 by Image Metrology).

The surface chemical composition before and after the etching process was measured by X-ray photoelectron spectroscopy (XPS). The measurements were performed at room temperature in an ultra-high vacuum system with a base pressure below 2×10^{-10} mbar equipped with a hemispherical electron energy analyser, nine channeltrons (Phoibos 150, SPECS Surface Nano Analysis GmbH, Berlin, Germany) and a monochromated AlK_α X-ray source (XR 50 M, $h\nu = 1486.7$ eV) operating at 300 W. The analysed region at the surface has a diameter of ∼ 1 mm. The samples were inserted via a load lock directly after processing as received (either only laser-treated or with additional chemical cleaning). The elemental composition was determined by fitting all spectra using CasaXPS version 2.3.24 [24] with the algorithms implemented therein considering the electron analyser transmission function. For all spectra, a Shirley-type background correction was performed, and the elemental sensitivity factors that are based on the cross sections reported by Scofield [25] and taking into account an inelastic mean free path (IMFP) of the emitted electrons, which depends on their kinetic energy: IMFP proportional to $E_{kin}^{0.7414}$ [26], are considered.

Cross-sectional specimens for transmission electron microscopy (TEM) analysis were prepared by the focused ion beam (FIB) technique (Auriga CrossBeam FIB-SEM, Carl Zeiss Microscopy GmbH). The TEM lamellae were cut with a Ga ion beam at an acceleration voltage of 30 kV and beam currents of 8nA and then 600 pA (fine polishing). After the lift-out procedure, the lamellae were attached to TEM grids by local Pt deposition from a precursor and afterwards thinned to electron transparency with a Ga ion beam at acceleration voltages of 15, 4 and 2 kV and beam currents of 250 (then 80 pA), 20 and 20 pA, respectively. Bright-field TEM was performed using a Titan3G2 60–300 (FEI) operated at 300 kV acceleration voltage in combination with a with Gatan UltraScan 1000XP CCD camera, while EDX analyses were performed in scanning TEM mode and using a SuperX detector system.

Raman spectra were recorded in the range of 85–1500 cm^{-1} with a Labram HR Evolution system (Horiba Scientific) at an excitation wavelength of 532 nm and a maximum laser power of 10.7 mW that was reduced by a neutral filter to approx. less than 3 mW. A×100 objective was used for focussing the laser beam to a spot of 1 to 2 µm and collecting the scattered light from the sample. Areal Raman data obtained by the scanning option of the device are consistence to localized measurements taken within one spot. The spectra were acquired with a grating of 600 lines per mm using an acquisition time of 30 s. LabSpec 6 software was used to evaluate the raw spectra that were subject to base line correction as well as smoothing before graphing.

The size of the micelles of the microemulsion was determined by dynamic light scattering (DLS) using Zetasizer (Malvern) without diluting the cleaning solutions.

3. Results

The etching rate of the cleaning liquids were determined by 4-point probe measurements of the temporal change of copper film resistance which are deposited on silicon wafers. The achieved etching rate data includes surface modification, e.g. grown copper oxides, that reduces the copper film thickness effectively too. The conductivity values of the cleaning liquids were determined using a calibrated InLab 742 ISM probe. The micelles size distributions of the applied microemulsions were determined by DLS and are graphed in the SI. The size distributions were fitted to a Gaussian distribution that enables to extract the mean size of the micelles. The size distributions of the microemulsions are shown in figure S4. Water contents, pH values, solution conductivity, mean size of the microemulsion's micelles, and the etching rates of the cleaning liquids measured at 50 °C are given in Table 1.

An extraction mechanism for CuO cleaning with microemulsions has been proposed already [27]. Sodium dodecyl sulfate (SDS)–butanol-1–extractant–kerosene–water systems containing caproic acid and D2EHPA (sodium di-(2-ethylhexyl)phosphate) as extractants were used to leach nonferrous metals from oxide raw materials. This leaching mechanism is highly dependent on the structure of the respective microemulsion (MEs). It is also dependent on the water content as well

Table 1
Type, pH values, electrical conductivity, micelles size and etching rate of the utilised wet-cleaning formulations. Reduced etching rates can be expected for the experimentally applied 25 °C etching temperature [21]. TECH Grade: technical quality; VLSI Grade: microelectronic quality.

Sample	pH-value	Etching rate @50 °C [nm/min]	Conductivity [µS/cm]	Water content [%]	Mean micelles size [nm]	Cleaning agent
19-UV	12.1	1.3	373	39	1.8	PG 5131 – TECH Grade from intelligent fluids GmbH
J-GZ	6.2	0.9	584	32	4.2	PS 3131 – TECH Grade from intelligent fluids GmbH
1O-XN	10.8	0.5	2840	43	13.8	R&D prototype from intelligent fluids GmbH
1L-2PJ	5.2	2.1	971	30	2.9	PS 3103 – TECH Grade from intelligent fluids GmbH
K-UV	6.3	0.03	2344	31	1.1	EC 4142 – TECH Grade from intelligent fluids GmbH
1L-2XV	5.1	0.01	2	29	1.7	PS 3003 – VLSI Grade from intelligent fluids GmbH
ISO	n.a.	0.01	0.21	50	n.a.	50 % Isopropanol / 50 % H_2O
NGL	9.3	0.33	n.a.	n.a.	n.a.	GP 17.40 SUP from NGL group

as on the conductivity. However, the ingredients of the herein utilized formulations are not altered in a homologous way. Therefore, a correlation between the effect of single ingredients and the conductivity and/or water content cannot be observed. However, a correlation between conductivity and etching rate of two homologous samples were identified: Sample 1L-2PJ and Sample 1L-2XV contain comparable ingredients in similar amounts. Both samples differ in purity, i.e. TECH grade (technical quality) and VLSI grade (microelectronic quality). VLSI grade is obtained by treatment of the ingredient formulation using an ion exchanger resin. This resin reduces conductivity and, therefore also reduces the respective etching rate of sample 1L-2XV compared to sample 1L-2PJ significantly. This finding is in line with typically described etching mechanisms for MEs [21].

It is clear from the applied pulse number that LIPSS formation is a multi-pulse phenomenon; hence the feedback from already available LIPSS by scattering processes determines the LIPSS period and their depth. This gradual increase in the LIPSS depth with the applied pulse number must be related to material melting, material transport and ablation processes, whereas parts of the ablated material are redeposited in the form of particles and debris. A prolonged irradiation of partially formed LIPSS with debris on top probably causes a mixing of these components near surface with the formation of various components and interfaces. The SEM images in Fig. 2 show the reference morphology of the copper samples after the LIPSS fabrication without any cleaning. The LIPSS period has been determined from the SEM images to be (360 ± 30) nm. Most of the redeposited particles are located between the laser tracks. Keeping in mind the spot diameter of 28 μm and the laser line distance of 10 μm, one has to consider that during continuous scanning, the interaction region is already partially covered with redeposited particles from the previous passage of the scanned laser spot that occurred at a distance of only 10 μm. These particles represent on one hand multiple scattering centres for the laser light, and, on the other hand, they shield the underlying Cu surface from direct photon irradiation. Both effects favour the formation of irregular surface structures and provoke that the LIPSS patterns of neighbouring scan lines are not in phase with the previously formed LIPSS, which results in the generation of bifurcations, local variations of the periodicity, and other defects in the periodic structure. The higher density of morphological distortions in the regions of lower light intensity are especially visible after removal of the particles (see Fig. 3). Thus, to optimise the LIPSS formation process, one should process in a regime of laser parameters where only little redeposition of particles occurs (at lower fluence) and one should adapt the hatch distance to the laser spot size. Nonetheless, a uniform LIPSS formation with suppressed particle formation is unlikely for processing larger areas as small variations in sample properties and processing parameters can easily influence the surface transformation processes. However, this was not the aim of our study for which we intentionally generated samples with particles.

The LIPSS samples that were fabricated with identical laser treatment parameters, underwent cleaning procedures with different wet-chemical solutions as listed in Table 1. We have tested two different cleaning durations to evaluate temporal influences. After SEM pre-characterisation at two magnifications, selected samples were furthermore investigated by AFM to determine the shape and the height of the LIPSS.

The SEM images in Fig. 3 show the most promising results for cleaning of LIPSS by different cleaning solutions that do not induce a strong etching effect. The reduction of the particle density is evident in the high-resolution images especially for 35 min of cleaning. In the low-resolution images, the particles only appear as bright pixels while the laser tracks can be identified. At higher magnification, the particle density and the cleaning efficacy can be better assessed. Fig. 3 highlights that particulate removal was achieved while the LIPSS pattern remained after 35 min treatment using mixtures 19-UV and J-GZ, while a shorter cleaning time is not as effective. One could speculate that the tiny depressions across the ripple surface (high-magnification SEM images), that exist after cleaning, are caused by local etching of the regions where originally the spherical particles are in contact with the LIPSS structure of the Cu surface. The observed features resemble structures formed by pit-etching during local corrosion [28]. SEM images of all other cleaning results are shown in Figure S1 of the supplementary material. Such an increase of the surface roughness was also observed for microemulsion etching of copper although the roughness increment is lower compared to aqueous etchants [21].

The characterisation by SEM does not allow to precisely measure the shape and the depth of the LIPSS grooves prior and after etching. Therefore, AFM measurements were performed to evaluate the surface roughness, the peak-to-valley height (P-V) of the ripples as well as the shape of LIPSS. The topographies of the as-processed surface and after cleaning with solutions 19-UV and 10-XN are shown in Fig. 4 a–c). A representative topography profile perpendicular to the ripples of the sample cleaned by solution 19-UV is shown in d). Such linear profiles were extracted for all samples and were then fitted by a sinusoidal function (see red-dotted example in d)) to extract the peak-to-valley (P-V) height of the LIPSS after cleaning. The − height is plotted in Fig. 4 e) for all cleaning solutions together with the χ^2 coefficient that indicates the fit quality. Both, the existing irregularities in the LIPSS pattern prior cleaning as well as laterally inhomogeneous etching effects cause deviations of the surface profile from a perfect sinusoidal function, which is represented by χ^2. In principle two classes of solutions can be

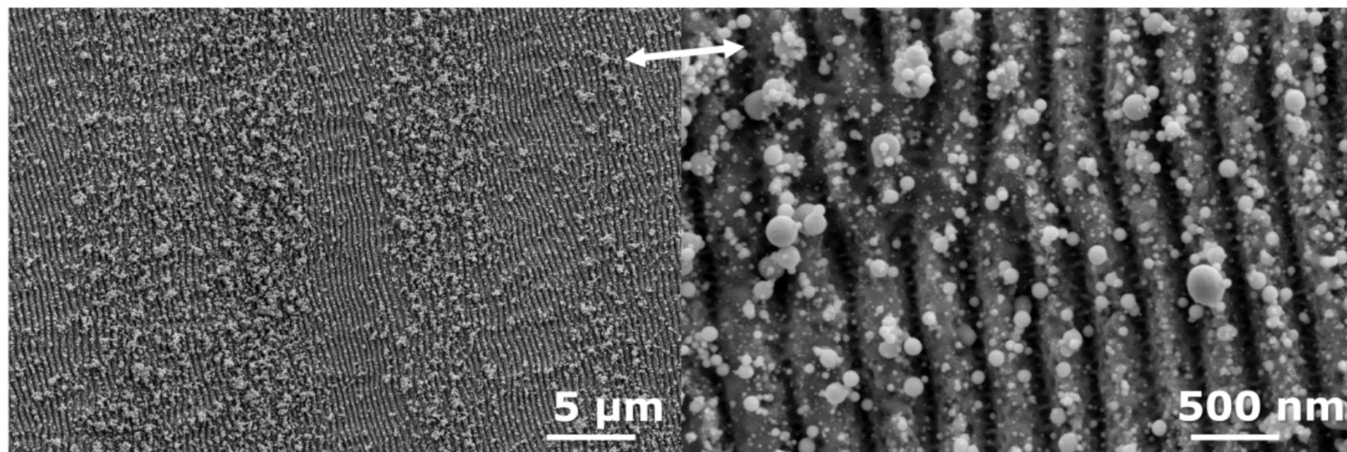

Fig. 2. Scanning electron micrographs of a copper surface after LIPSS fabrication at two different magnifications. In addition to the linear LIPSS pattern with a lateral periodicity of ~ 365 nm, various debris, and particulate contaminations such as spherical Cu droplets can be found. The double arrow indicates the laser polarisation direction.

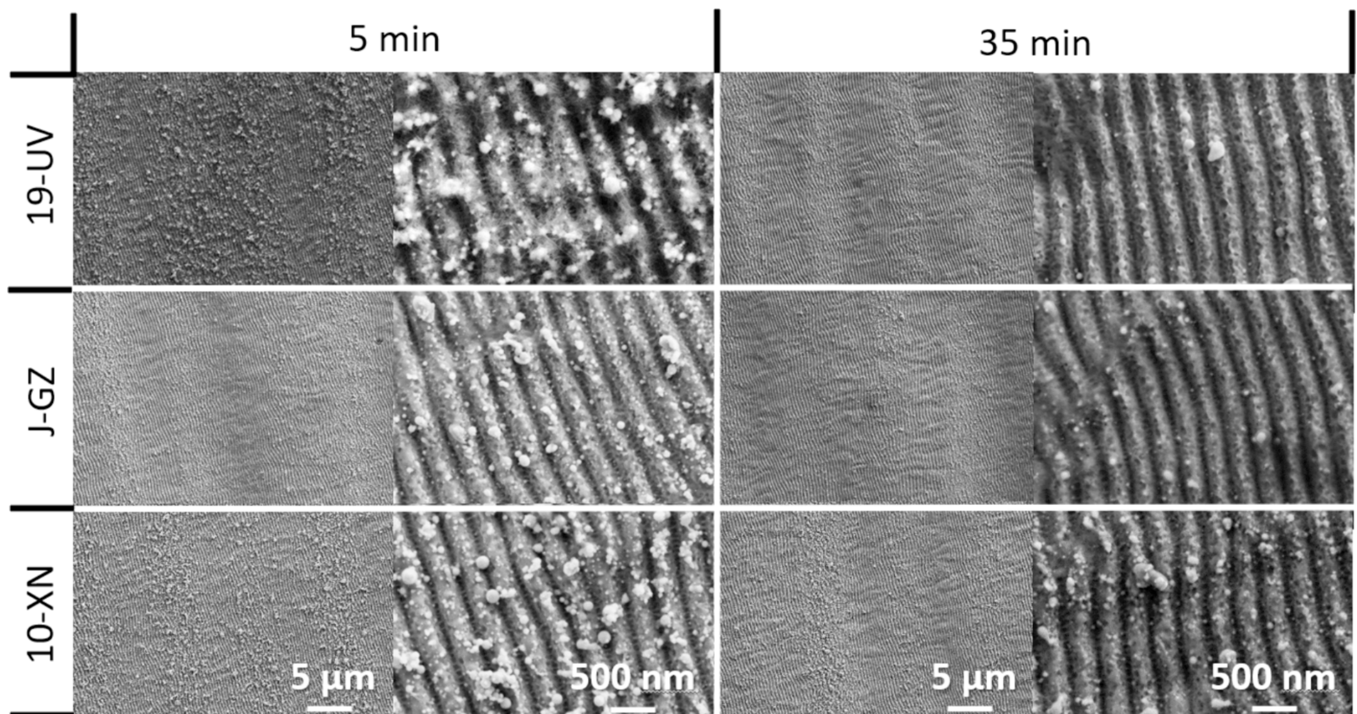

Fig. 3. Scanning electron micrographs of the copper surfaces with LIPSS after wet-chemical cleaning with the three most promising cleaning solutions at two different cleaning durations.

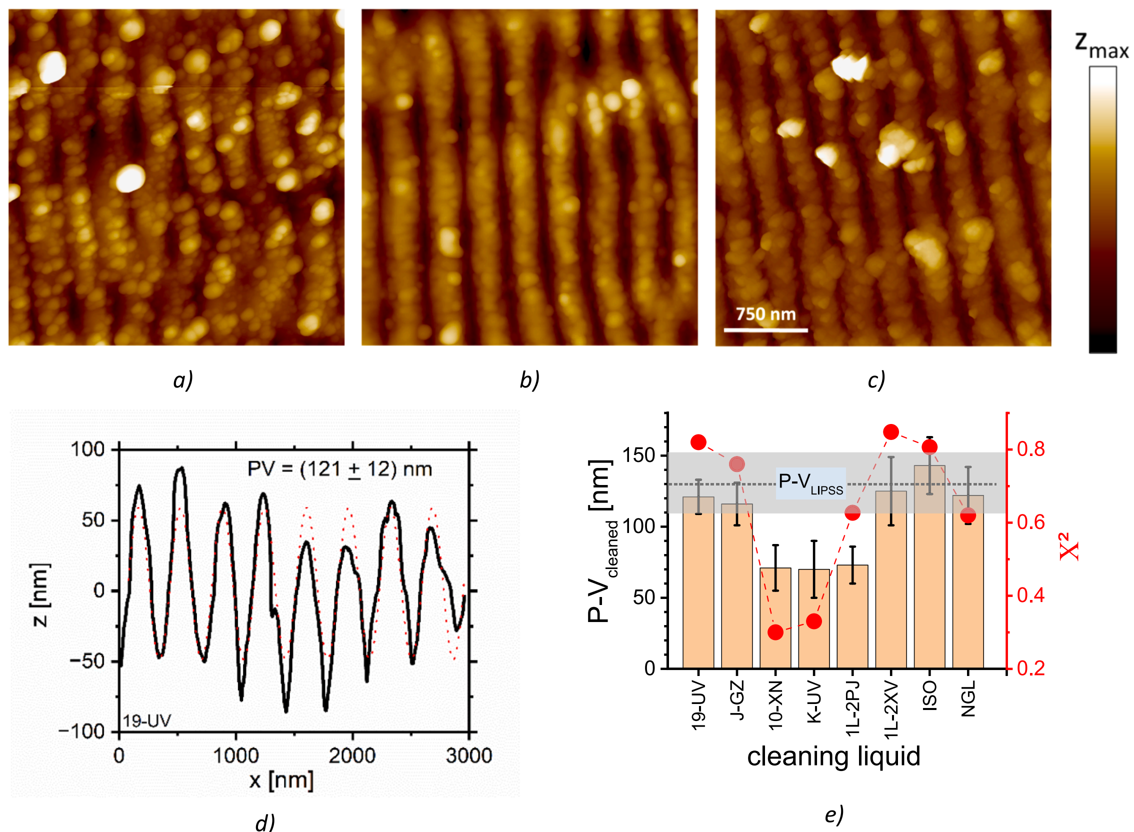

Fig. 4. Selected results of the AFM studies: a) reference surface and cleaned for 30 min with b) 19-UV, and c) 10-XN solution, respectively. The colour scale is z_{max} = 500 nm. d) Surface topography profile perpendicular to the LIPSS after cleaning with the solution 19-UV. In addition to the measured data, a fitted sinusoidal function is plotted as red dotted profile. e) Peak-to-valley height of the LIPSS after cleaning with the different solutions. The results can be classified in two groups of cleaning solutions: one group causes the reduction of the P-V height due to severe etching of the ripples, whereas the other group of solutions does not induce an alteration of the Response R2(7): P-V value. Further AFM measurements with the corresponding cross sections are shown in Figure S3.

distinguished: (i) mixtures that do not change the shape, the height, and the aspect ratio of the ripples and (ii) mixtures that strongly etch the Cu surface and thereby reduce the P-V height and shape of the LIPSS. It must be noticed that a certain correlation between the LIPSS P-V height and their pattern quality, quantified by the χ^2 value, can be identified. Hence, once the LIPSS surface is etched, substantial changes of the ripple shape can be expected. On the other hand, the higher χ^2 values of the 19-UV and 1L-2XV samples can be due to the removal of particles on top of the ripples, which otherwise represent distortions from a perfect pattern.

To further characterise the LIPSS with the remaining particles, cross-sections were prepared by FIB and post-polished by low energy ion polishing at glancing incidence. The cross-sections were transferred to the TEM without protection for imaging. TEM cross section images of the most relevant samples are compared in Fig. 5b. The copper LIPSS cleaned with ISO exhibit an identical particle density as samples after laser processing. Some of the particulates are molten to the copper surface while others are attached to the LIPSS surface via a thin oxide/mixed layer. Oxide phases exist at the top of the LIPSS surface as well as at the surface of attached particles. The shape of the LIPSS before and after cleaning with solutions 19-UV and 1L-2XV are almost similar. Differences in shape can be attributed to irregularities/defects of the LIPSS structure. Therefore, shape changes due to the cleaning process cannot be reported with sufficient confidence. EDX studies of the cleaned surface in the TEM proved the coverage with a thin oxide layer after wet cleaning.

The alteration of the amplitude of the LIPSS after the cleaning procedures points to possible surface etching processes induced by some of the cleaning mixtures that can be supported by the ultrasonication process. Therefore, the surface composition was examined. X-ray photoelectron spectra of the laser-processed surfaces with and without cleaning are shown in Fig. 6, which allow insight into the surface composition induced by the focussed laser beam as well as into the changes and processes provoked by the different chemical solutions during cleaning. The spectra after laser processing in air are identical to earlier studies on LIPSS formation for SEY (secondary electron yield) reduction: the surface is partially oxidised and contains surface hydroxide bonds and hydrocarbon adsorbates [4,23]. The surface elemental composition can be quantified with a simplified model of homogeneous distribution of all detected elements that typically overestimates contribution from the outermost surface layers. The result of this analysis is shown in Table 2. The reference cleaning with NGL detergent slightly attacks the surface chemically (Cu etching rate of ~20 nm/hour). Consequently, the amount of surface carbon adsorbates is reduced, and the oxidation degree is lower. The surface remains partially metallic, partially oxidised (Cu_2O) with a rather low degree of formed surface hydroxide states [29]. The state in the O 1 s spectrum at 530.3 eV corresponds to the Cu–O bonds of the Cu_2O surface oxide [30], while the second feature at 531.5 eV includes a superposition of surface hydroxide bonds and oxygen atoms in adsorbed hydrocarbon molecules. The other cleaning solutions have different effects on the surface composition of the Cu LIPSS surface, while no clear correlation of the XPS data with the found etching of the ripples (see Fig. 4) can be identified. Most of the liquid treatments add a remarkable degree of adsorbed hydrocarbon molecules to the surface and some of them also lead to strong uptake of nitrogen at the surface (see Fig. 6 and Table 2). Especially for samples *J-GZ*, *10-XN*, and *1L-2XV* a high carbon content > 60 at. % remains at the surface. The shift of the main C 1 s peak to higher binding energy between those three samples indicates a successively increasing polarity of the carbon-containing adsorbates at the surface of the cleaned samples. This is especially evident for the sample *J-GZ* for which also additional chemical states are detected in the C1s spectrum around 286.3 eV and in the O 1 s spectrum at 532.8 eV. Another sample with different molecular structure of the carbon adsorbates is the one treated with *1L-2PJ*, which exhibits an additional feature at 286.1 eV in the C 1 s spectrum besides the common states at ~ 284.9 and ~ 288.5 eV caused by airborne adsorption. Furthermore, samples *10-XN* and *1L-2XV* not only exhibit a high nitrogen content at a N 1 s binding energy of ~ 400.0 eV. The change in the Cu LMM spectrum and the appearance of a spectral signature at 914.8 eV kinetic energy indicate the formation of Cu–CN bonds [31], i.e. a chemical transformation of the copper surface induced by the constituents of the cleaning solution. Finally, the adsorbate content of the sample *1L-2PJ* is comparatively low and closest to the composition of the LIPSS reference sample.

Raman spectra were taken from pristine, LIPSS-modified and cleaned LIPSS copper surfaces. Raman spectra with a meaningful signature of copper compounds were only acquired from LIPSS that were not cleaned as is shown in Fig. 7.

Only small signatures of copper oxide (Cu_2O) around 100 cm^{-1} are found for pristine copper samples. Very similar spectra were acquired from LIPSS surfaces cleaned with the solutions IL-2PJ and 19-UV. Contrary LIPSS-modified copper feature a significant peak signature that can be assigned to different types of copper oxide. The peaks centred around 296, 346, and 631 cm^{-1} are typical for CuO [32,33] but additional peaks can appear depending on the oxidation process [34]. Cu_2O peaks

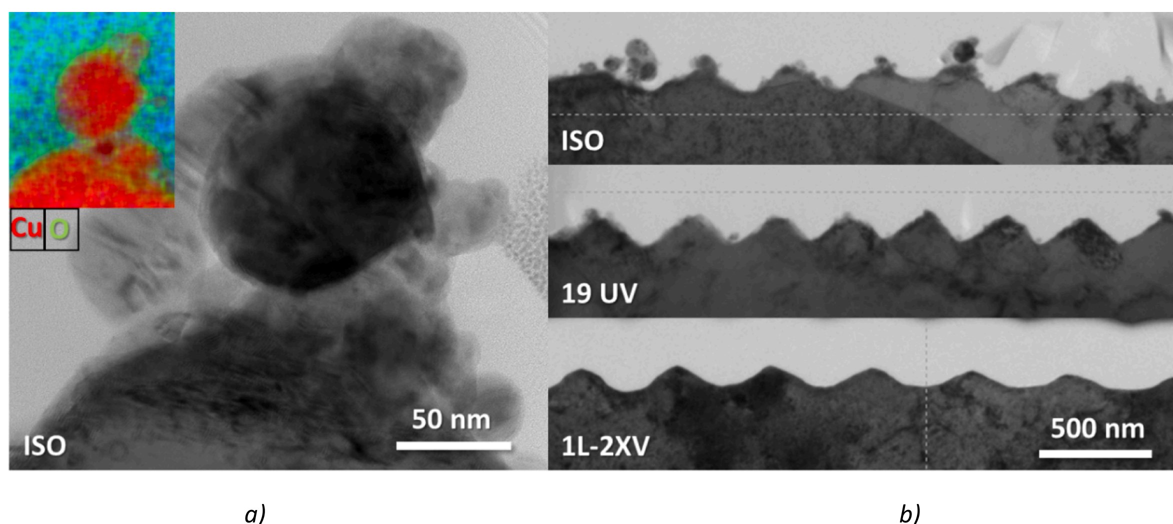

Fig. 5. TEM images of selected samples. a) Adherent particles on top of the LIPSS ripple pattern. The image as well as the colour-coded inset show the multiphase composition of the interface region. b) Comparison of cross-sections for not cleaned (ISO) and cleaned (19 UV, 1L-2XV) LIPSS at copper surfaces. The reduction of the particle density as well as the almost unchanged shape of the LIPSS are visible.

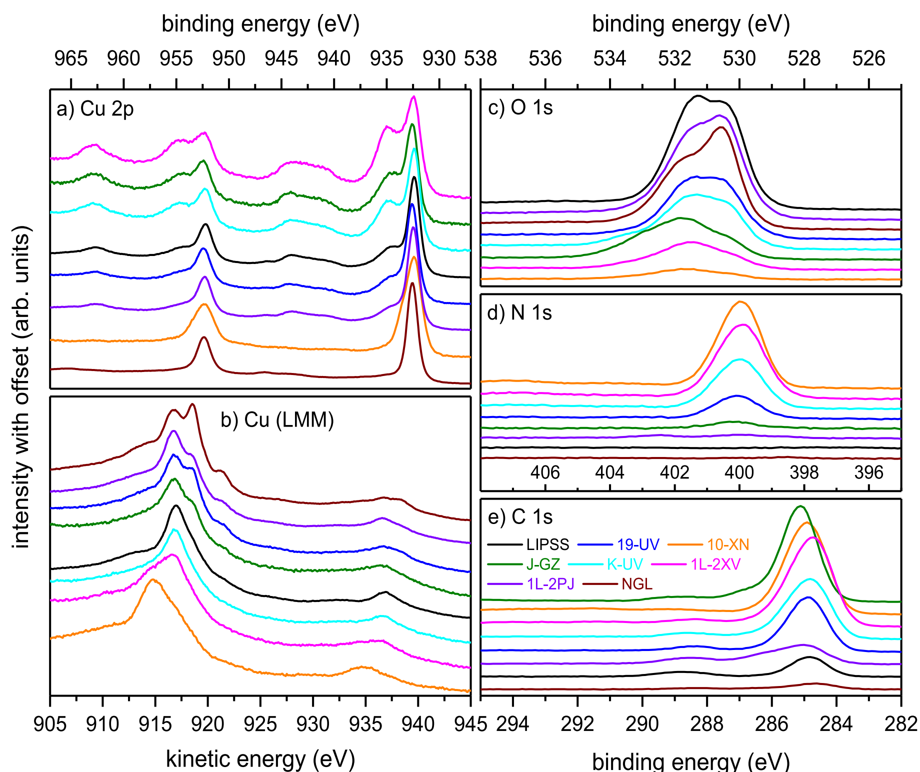

Fig. 6. Selected XPS spectra of the Cu samples after LIPSS processing as well as with subsequent chemical cleaning as indicated in the legend: a) Cu 2p state, b) Cu (LMM) Auger excitation, c) O 1 s state, d) N 1 s state and e) C 1 s state.

Table 2
Surface composition (in at.%) based on the quantitative XPS analysis for Cu surfaces after laser treatment and after further chemical cleaning. The Si uptake as indicated (*) is due to a constituent of the NGL detergent and typically remains present after rinsing.

sample	C	Cu	N	O	Si
LIPSS	19.2	47.4	0.6	32.7	–
19-UV	44.6	30.3	6.6	18.6	–
J-GZ	67.6	13.3	1.4	17.7	–
10-XN	64.5	12.1	19.6	3.8	–
K-UV	51.5	19.1	12.2	17.2	–
1L-2PJ	25.3	44.4	1.7	28.5	–
1L-2XV	61.7	11.6	16.1	10.5	–
NGL	6.8	61.6	0.4	26.3	4.9*

are located around 150, 415, 525, and 623 cm^{-1} whereas the sharpest line is centred at 220 cm^{-1} [33,34]. Different copper oxide modifications regarding the composition, the defect density as well as the crystal size can contribute to the broad peaks around 530 and 615 cm^{-1}. The broad peak around 530 cm^{-1} can be assigned to Cu_2O (≈525 cm^{-1}) or Cu_4O_3 (530 cm^{-1}) whereas the peak at 615 cm^{-1} can be mainly related to Cu_2O. Cu_3N that exhibits a peak at 655 cm^{-1} was not found [33,35]. Similar Raman lines centred at 91, 142, 214, 520, and 629 cm^{-1} were reported for ps-laser LIPSS formation at copper surfaces in air [23]. After thermal oxidation of copper foils, Raman lines at 100, 151, 220, 308, and 643 cm^{-1} were observed [36].

A summary of the cleaning results in terms of effectiveness to remove particles in relation to the preservation of LIPSS shape/height is given in Table 3.

4. Discussion

The efficiency and the quality of cleaning particle-covered LIPSS structures at copper surfaces by wet processing depends strongly on the

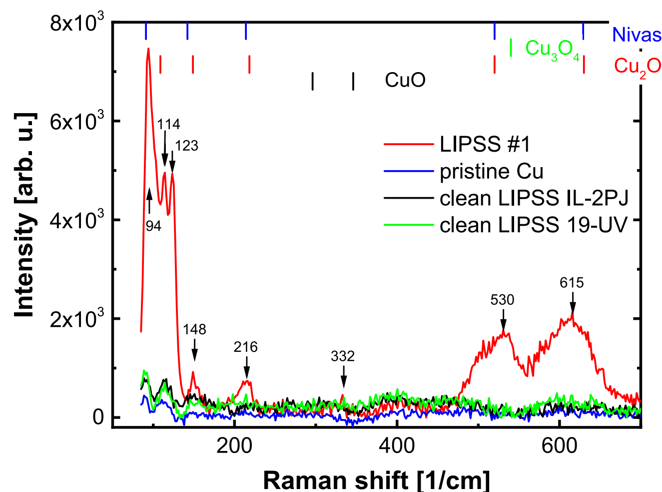

Fig. 7. Raman spectra of different surfaces of cleaned and not cleaned copper samples.

utilised cleaning solution. The reduction of the P-V value as well as the shape changes of the LIPSS are strong indications that gentle etching processes occur during cleaning. Contrary to the expectations, a strong correlation between cleaning efficiency and the etching rate could not be found. This can be related to the more complex structure and chemical composition of surface and subsurface after LIPSS formation that shows a rather three-dimensional mixture of metallic and oxidized copper phases in comparison with pristine copper. Furthermore, the ultrashort pulse laser irradiation can result also in structural changes of materials such as amorphization [37]. The size of the micelles determined by DLS varies with the particular composition of the microemulsion in the range of 1 to 15 nm but this size is much smaller than the

Table 3
Summary of the cleaning results in relation to the evaluated cleaning efficiency, the alteration of the LIPSS shape, and the amplitude of the remaining LIPSS.

Etching/cleaning	time		P-V [nm]	Particles cleaning efficiency
solution	5 min	35 min	@ 35 min	no or very weak
19-UV		W	120.8	weak to medium
J-GZ		W	116	medium
1O-XN		W	70.5	good
K-UV		W	70.2	very good
1L-2PJ	**W**	**S**	73.4	
1L-2XV		**W**	124.6	LIPSS shape alterations
ISO				**W**eak
NGL			75	**S**trong

period of the LIPSS as well as the particles of the debris (see Fig. 2 and Fig. 5 as well as the images in the Supplementary Information. A relation of the micelles size of the microemulsion and the cleaning quality cannot be ascertained. In this relation, the physical properties of the cleaning liquid such as the surface tension or the viscosity as well as the chemical interactions can be considered as homogeneous. Hence, changes of the LIPSS amplitude, or the P-V value, the removal of particulate contaminations from a surface using microemulsions and the related alterations of the surface composition is a complex process and differs from simple thin film etching with known removal rate.

To achieve the goal of a selective removal of particulates without deteriorating the LIPSS, the P-V height and the shape needs to be maintained during cleaning. The results presented in Fig. 4 can be discussed in terms of etching processes that influence both the removal process of particulates as well as partial etching of the LIPSS. The reduction of the P-V height and alteration of the LIPSS-shape (given by the χ^2 values) found for some cleaning solutions can be related to isotropic etching processes. Particulates are removed by wet-cleaning of the LIPSS surface if a local etching in the contact region between particulate and substrate occurs and if the surfactants subsequently support the particle detachment. Solutions that maintain the LIPSS P-V height must show selective, inhomogeneous etching that prefers small particles on the top of the LIPSS. Considering the composition of the microemulsion systems that contain surface active molecules and etchants, it can be suggested that the inhibition effects of surfactant molecules depend on the surface morphology, where small peaks of a topography or particles with low surface coverage etch faster than the large undulations of the LIPSS structure.

The particle density was determined from SEM top view images using the processing software SPIP® for the three samples. The areal particle densities calculated from the SEM images for the samples without cleaning and cleaned with 19-UV and 1O-XN are 17 %, 4.7 %, and 5.6 %, respectively, allowing a quantitative comparison of the cleaning efficiency.

A clear correlation between the etching rate and the alteration of the amplitude of the cleaned LIPSS was not found. This suggests a more complex etching mechanism for LIPSS in comparison to thin film etching, where only a homogeneous surface oxidation of the copper can be expected [38,39]. The oxide layer on LIPSS that is with approx. 20 nm (see TEM in Figure S3) much thicker than that of copper film (several nm thickness [38,39]) give evidence for different etching effects. As the etching rate is sensitive to morphology, structure, or surface composition, it is not identical when comparing thin films and LIPSS structures. For instance, particles are bonded to the surface of the LIPSS via oxidized copper; the preferential etching of copper oxides can cause the detachment of those particles without significantly etching of the metallic copper LIPSS structures underneath. On the other hand, without a sufficient selectivity of etching, both the particles and the LIPSS structures are etched. In Ref. [21] a feature-size dependent selective etching is discussed where the droplet size of the microemulsion defines the size of enhanced etching. In addition, microemulsions etch more easily protrusions than pores or grooves. Consequently, their complex composition and the included surfactants play an important role to realize the selective removal of small surface contaminations.

The TEM and AFM images after cleaning with 19-UV and 1L-2XV show almost the same LIPSS P-V-height as before cleaning. It seems, that the shape of the LIPSS slightly changed, i.e. the originally rounded peaks and valleys of the periodic structures exhibit a profile with sharper edges. Further, in the high-resolution TEM images of all studied copper samples, a coverage by crystalline oxides has been observed. The thickness is in the range of 2 nm, except the uncleaned LIPSS-sample that has a varying oxide thickness of more than 10 nm.

These oxides at the uncleaned LIPSS have been clearly seen by Raman spectroscopy. The composition of the oxides that are located at the copper surface as well as at the redeposited particulates is inhomogeneous and probably includes Cu_2O and CuO. The mechanism of oxide growth on copper comprises first an oxidation to Cu_2O that will be oxidized further to CuO for elongated oxidation times [30,38,39]. The Raman spectra suggest a thermal oxidation of the irradiated copper surface as well as the ablated particles that are redeposited, which can be explained by the laser-induced heating of the Cu surface and the oxidation of ablated copper.

On the other hand, the cleaned surfaces show as well as the pristine samples very week Raman peaks related to oxides. In agreement, only a thin oxide layer was observed in the EDX/TEM studies. Most probably these oxides can be related to the formation of a native oxide after wet cleaning, but oxidation processes during the cleaning process may be involved too.

In this context, it is necessary to consider the XPS data pertaining to the etched surfaces. The higher C1s peaks of the etched surfaces suggest remaining carbon contaminations that likely consist of adsorbed surfactants originating from the wet cleaning solution.

Mechanism of particulate removal cannot be explained in all cases simply by etching of the particles at top of the LIPSS, as its ripple surface is also etched at the same time. However, the increased removal efficiency with time and the slight change of the LIPSS shape indicate a rather slow surface etching process. Despite that, surface charging by constituents of the cleaning liquid cannot be completely excluded as this effect typically occurs very quickly. The complex structure of the attached particles (see Fig. 5 and Figure S3) especially at the interface to the LIPSS suggest a localised etching mechanism. Therefore, it is likely that the complex composed surface of the particulates is etched also at the interface to the LIPSS and with the etching the interface the particles detach and are dissipated in the liquid by the ultrasonic agitation.

5. Conclusions

Ultrashort pulse laser fabricated LIPSS on copper samples contaminated by particular debris were subject to wet-chemical cleaning processes using different solutions to remove redeposited particles and debris that originate from the ablative LIPSS formation process. The investigated cleaning liquids have different particulate removal efficiencies but also influence the shape and height of the wet-cleaned LIPSS according to the cleaning/etching mechanism. Hydrocarbon solvents also with ultrasonication have no cleaning effect. High etching rates (1L-2PJ) provide good cleaning capabilities but cause severe LIPSS shape modifications. The utilized microemulsions provide low copper etching rates and obviously feature a selective, localized etching, e.g. of oxides and nano-sized debris. In contrast to isotropic etching such characteristics of a cleaning liquid enable the removal of laser debris that comprise copper particles fixed at the surface and copper oxides but preserving copper submicron structures like LIPSS. As microemulsions enable both etching of the metallic copper as well as selective and localized etching of modified copper, e.g. oxidized, debris, or nanostructures, the composition of the microemulsion must fit to the characteristics of the surface to be cleaned and the goals of the cleaning, e.g. maintaining micron pattern. The LIPSS periodicity is, as expected, not changed by the cleaning procedure. The best suited solutions maintain

the shape of the LIPSS, which proves a limited isotopic etching of the copper substrate surface. However, the efficient removal of particular debris is a strong indication of localized, selective etching of nano-structured copper modifications. In relation to cleaning LIPSS on copper sheets the mixture 19-UV as well as 1L-2XV seem to be best suited. The selective removal of particles enables the quantification of LIPSS exclusively which can be helpful to study the impact of particles to the formation of LIPSS defects such as local changing period or bifurcations.

CRediT authorship contribution statement

Pierre Lorenz: Visualization, Investigation, Formal analysis. **Martin Ehrhardt:** Investigation. **Andriy Lotnyk:** Visualization, Methodology, Investigation. **Jan Griebel:** Formal analysis, Investigation. **Klaus Zimmer:** Writing – review & editing, Writing – original draft, Supervision, Conceptualization. **Joachim Zajadacz:** Writing – original draft, Investigation. **Marcel Himmerlich:** Writing – review & editing, Visualization, Methodology, Investigation, Formal analysis. **Elena Bez:** Writing – review & editing, Investigation. **Mauro Taborelli:** Writing – review & editing, Supervision. **Steffen Rosenow:** Investigation. **Ronny Tepper:** Methodology, Investigation. **Alexander Max Breul:** Writing – review & editing, Writing – original draft, Supervision, Methodology, Formal analysis.

Declaration of competing interest

The authors declare that they have no known competing financial interests or personal relationships that could have appeared to influence the work reported in this paper.

Data availability

Data will be made available on request.

Acknowledgements

The authors thank A. Mill for the preparation of TEM lamellae by FIB and I. Mauersberger for the help in SEM and AFM imaging. The authors acknowledge L. Stieler for performing the DLS measurements.

Appendix A. Supplementary data

Supplementary data to this article can be found online at https://doi.org/10.1016/j.apsusc.2024.161115.

References

[1] J. Bonse, S. Höhm, S.V. Kirner, A. Rosenfeld, J. Krüger, Laser-induced periodic surface structures—a scientific evergreen, IEEE J. Sel. Top. Quantum Electron. 23 (2016).
[2] B. Ziberi, F. Frost, T. Hoche, B. Rauschenbach, Ripple pattern formation on silicon surfaces by low-energy ion-beam erosion: experiment and theory, Phys. Rev. B 72 (2005) 7, https://doi.org/10.1103/PhysRevB.72.235310.
[3] P. Lorenz, et al., Secondary electron yield engineering of copper surfaces by 532 nm ultrashort laser pulses, Procedia CIRP 111 (2022) 662–666, https://doi.org/10.1016/j.procir.2022.08.017.
[4] J.J.J. Nivas, et al., Secondary electron yield reduction by femtosecond pulse laser-induced periodic surface structuring, Surf. Interfaces 25 (2021) 101179, https://doi.org/10.1016/j.surfin.2021.101179.
[5] S. Maragkaki, et al., Wavelength dependence of picosecond laser-induced periodic surface structures on copper, Appl. Surf. Sci. 417 (2017) 88–92, https://doi.org/10.1016/j.apsusc.2017.02.068.
[6] T.T.D. Huynh, A. Petit, N. Semmar, Picosecond laser induced periodic surface structure on copper thin films, Appl. Surf. Sci. 302 (2014) 109–113, https://doi.org/10.1016/j.apsusc.2013.10.172.
[7] P. Lorenz, et al., Secondary electron yield reduction of copper after 355 nm ultrashort pulse laser ablation, Lasers in Manufacturing and Materials Processing (2022), https://doi.org/10.1007/s40516-022-00167-5.
[8] D. Zhang, R. Liu, Z. Li, Irregular LIPSS produced on metals by single linearly polarized femtosecond laser, International Journal of Extreme Manufacturing 4 (2022) 015102, https://doi.org/10.1088/2631-7990/ac376c.
[9] J. Bonse, S.T. Gräf, Open questions about laser-induced periodic surface structures, Nanomaterials 11 (2021), https://doi.org/10.3390/nano11123326.
[10] A. Braun, K. Zimmer, F. Bigl, The influence of ambient temperature on KrF laser ablation of polyimide in air, Appl. Surf. Sci. 154 (2000) 73–77, https://doi.org/10.1016/s0169-4332(99)00396-7.
[11] A.F. Sartori, et al., Laser-Induced Periodic Surface Structures (LIPSS) on heavily boron-doped diamond for electrode applications, ACS Appl. Mater. Interfaces 10 (2018) 43236–43251, https://doi.org/10.1021/acsami.8b15951.
[12] D.M. Knotter, The chemistry of wet cleaning, Handbook of Cleaning in Semiconductor Manufacturing: Fundamental and Applications (2010) 39–94.
[13] K. Qin, Y. Li, Mechanisms of particle removal from silicon wafer surface in wet chemical cleaning process, J. Colloid Interface Sci. 261 (2003) 569–574, https://doi.org/10.1016/S0021-9797(03)00053-5.
[14] C.D. Ohl, M. Arora, R. Dijkink, V. Janve, D. Lohse, Surface cleaning from laser-induced cavitation bubbles, Appl. Phys. Lett. 89 (2006), https://doi.org/10.1063/1.2337506.
[15] A.C. Tam, W.P. Leung, W. Zapka, W. Ziemlich, Laser-cleaning techniques for removal of surface particulates, J. Appl. Phys. 71 (1992) 3515–3523, https://doi.org/10.1063/1.350906.
[16] W. Zapka, W. Ziemlich, A.C. Tam, Efficient pulsed laser removal of 0.2 µm sized particles from a solid surface, Appl. Phys. Lett. 58 (1991) 2217–2219, https://doi.org/10.1063/1.104931.
[17] J. Huang, et al., Fabrication of highly homogeneous and controllable nanogratings on silicon via chemical etching-assisted femtosecond laser modification, Nanophotonics 8 (2019) 869–878, https://doi.org/10.1515/nanoph-2019-0056.
[18] Y.-C. Liang, et al., High-quality structures on 4H-SiC fabricated by femtosecond laser LIPSS and chemical etching, Opt. Laser Technol. 163 (2023) 109437, https://doi.org/10.1016/j.optlastec.2023.109437.
[19] E.W. Hoppe, et al., Cleaning and passivation of copper surfaces to remove surface radioactivity and prevent oxide formation, Nucl. Instrum. Methods Phys. Res., Sect. A 579 (2007) 486–489, https://doi.org/10.1016/j.nima.2007.04.101.
[20] L. Zhang, T. Wang, X. Lu, The effect of citric acid based cleaning solution on particle adhesion and removal during post-Cu CMP cleaning, Microelectron. Eng. 216 (2019) 111090, https://doi.org/10.1016/j.mee.2019.111090.
[21] Y.J. Huang, M.Z. Yates, Copper etching by water-in-oil microemulsions, Colloids Surf A Physicochem Eng Asp 281 (2006) 215–220, https://doi.org/10.1016/j.colsurfa.2006.02.041.
[22] Stubenrauch, C. *Microemulsions: Background, New Concepts, Applications, Perspectives*. 375 (Wiley, 2009).
[23] J.J. Nivas, et al., Laser-induced periodic surface structuring for secondary electron yield reduction of copper: dependence on ambient gas and wavelength, Appl. Surf. Sci. 622 (2023) 156908, https://doi.org/10.1016/j.apsusc.2023.156908.
[24] N. Fairley, et al., Systematic and collaborative approach to problem solving using X-ray photoelectron spectroscopy, Applied Surface Science Advances 5 (2021) 100112, https://doi.org/10.1016/j.apsadv.2021.100112.
[25] J.H. Scofield, Hartree-Slater subshell photoionization cross-sections at 1254 and 1487 eV, J. Electron Spectrosc. Relat. Phenom. 8 (1976) 129–137, https://doi.org/10.1016/0368-2048(76)80015-1.
[26] A. Jablonski, Universal energy dependence of the inelastic mean free path, Surf. Interface Anal. 20 (1993) 317–321, https://doi.org/10.1002/sia.740200409.
[27] N.M. Murashova, A.S. Polyakova, Effect of the structure of water-in-oil microemulsions of sodium Di-(2-ethylhexyl)phosphate and sodium dodecyl sulfate on the efficiency of microemulsion leaching of copper, Colloid J. 86 (2024) 98–108, https://doi.org/10.1134/S1061933X2360104X.
[28] J. Li, D. Lampner, In-situ AFM study of pitting corrosion of Cu thin films, Colloids Surf A Physicochem Eng Asp 154 (1999) 227–237, https://doi.org/10.1016/S0927-7757(98)00901-7.
[29] M.C. Biesinger, Advanced analysis of copper X-ray photoelectron spectra, Surf. Interface Anal. 49 (2017) 1325–1334, https://doi.org/10.1002/sia.6239.
[30] S. Poulston, P.M. Parlett, P. Stone, M. Bowker, Surface oxidation and reduction of CuO and Cu2O studied using XPS and XAES, Surf. Interface Anal. 24 (1996) 811–820, https://doi.org/10.1002/(SICI)1096-9918(199611)24:12<811::AID-SIA191>3.0.CO;2-Z.
[31] C.D. Wagner, Chemical shifts of auger lines, and the auger parameter, Faraday Discuss. Chem. Soc. 60 (1975) 291–300, https://doi.org/10.1039/DC9756000291.
[32] L. Debbichi, M.C. Marco de Lucas, J.F. Pierson, P. Krüger, Vibrational properties of CuO and Cu4O3 from first-principles calculations, and raman and infrared spectroscopy, J. Phys. Chem. C 116 (2012) 10232–10237, https://doi.org/10.1021/jp303096m.
[33] K. Mavridou, M. Zervos, F. Pinakidou, M. Brzhezinskaya, M. Katsikini, Oxidation of Cu_3N thin films obtained from Cu annealed under NH_3:O_2 flow: a Raman and N-K-edge NEXAFS study, J. Alloy. Compd. 914 (2022) 165293, https://doi.org/10.1016/j.jallcom.2022.165293.
[34] Y. Deng, A.D. Handoko, Y. Du, S. Xi, B.S. Yeo, In situ raman spectroscopy of copper and copper oxide surfaces during electrochemical oxygen evolution reaction: identification of cuiii oxides as catalytically active species, ACS Catal. 6 (2016) 2473–2481, https://doi.org/10.1021/acscatal.6b00205.
[35] K. Nowakowska-Langier, et al., Phase composition of copper nitride coatings examined by the use of X-ray diffraction and Raman spectroscopy, J. Mol. Struct. 1165 (2018) 79–83, https://doi.org/10.1016/j.molstruc.2018.03.107.
[36] A. Gergely, A review on corrosion protection with single-layer, multilayer, and composites of graphene, Corros. Rev. 36 (2018) 155–225, https://doi.org/10.1515/corrrev-2017-0016.

[37] T.P. Remington, B.A. Remington, E.N. Hahn, M.A. Meyers, Deformation and failure in extreme regimes by high-energy pulsed lasers: a review, Mater. Sci. Eng. A 688 (2017) 429–458, https://doi.org/10.1016/j.msea.2017.01.114.

[38] J.-W. Lim, et al., Nanoscale investigation of long-term native oxidation of Cu films, Thin Solid Films 516 (2008) 4040–4046, https://doi.org/10.1016/j.tsf.2007.12.159.

[39] J. Iijima, et al., Native oxidation of ultra high purity Cu bulk and thin films, Appl. Surf. Sci. 253 (2006) 2825–2829, https://doi.org/10.1016/j.apsusc.2006.05.063.